Published in final edited form as:

Nature. 2017 December 14; 552(7684): 253–257. doi:10.1038/nature24993.

Runx3 programs CD8+ T cell residency in non-lymphoid tissues and tumors

J. Justin Milner[1], **Clara Toma**[1,8], **Bingfei Yu**[1,8], **Kai Zhang**[2], **Kyla Omilusik**[1], **Anthony T. Phan**[1], **Dapeng Wang**[3], **Adam J. Getzler**[3], **Toan Nguyen**[1], **Shane Crotty**[4,5], **Wei Wang**[2,6,7], **Matthew E. Pipkin**[3,*], and **Ananda W. Goldrath**[1,*]

[1]Division of Biological Sciences, University of California, San Diego, La Jolla, California, USA

[2]Bioinformatics and Systems Biology Graduate Program, University of California, San Diego, La Jolla, California, USA

[3]Department of Immunology and Microbial Science, The Scripps Research Institute, Jupiter, Florida, USA

[4]Division of Vaccine Discovery, La Jolla Institute for Allergy and Immunology, La Jolla, USA

[5]Division of Infectious Diseases, Department of Medicine, University of California, San Diego, La Jolla, California, USA

[6]Department of Chemistry and Biochemistry, University of California, San Diego, La Jolla, California, USA

[7]Department of Cellular and Molecular Medicine, University of California, San Diego, La Jolla, California, USA

Tissue-resident memory CD8$^+$ T cells (Trm) are positioned at common sites of pathogen exposure where they elicit rapid and robust protective immune responses[1,2]. However, the molecular signals controlling Trm differentiation and homeostasis are not fully understood. Here we show that mouse Trm precursor cells represent a unique CD8$^+$ T cell subset that is distinct from the precursors of circulating memory populations at the levels of gene expression and chromatin accessibility. Exploiting computational and functional RNAi *in vivo* screens, we identified the transcription factor (TF) Runx3 as a key regulator of Trm differentiation and homeostasis. Runx3 was required to establish Trm populations in diverse tissue environments and supported expression of critical tissue-residency genes while suppressing genes associated with tissue egress and recirculation. Analysis of the

*Correspondence should be addressed to M.E.P. (mpipkin@scripps.edu) or A.W.G. (agoldrath@ucsd.edu).
[8]These authors contributed equally to this work;

Author Contributions: J.J.M. designed and performed experiments, analyzed the data and wrote the manuscript; C.T. assisted with the RNAi screen, transfections, transductions, tissue processing, and tumor models; B.Y. performed the computational analyses and ATAC-seq experiment; K.Z. assisted with computational analyses; K.O. assisted with tissue processing, analysis, and qPCR; A.T.P assisted with tissue processing, inducible deletion experiments, and analysis; D.W and A.J.G. helped with the inducible deletion experiments, RNA-seq analysis, and tumor models; S.C provided reagents and advice; W.W. supervised the computational analysis and contributed advice; M.E.P. and A.W.G. supervised the project, designed experiments, and wrote the manuscript.

Author Information: The authors declare no competing financial interests.

accessibility of Runx3 target genes in Trm-precursor cells revealed a distinct regulatory role for Runx3 in controlling Trm differentiation despite relatively widespread and uniform expression among all $CD8^+$ T cell subsets. Further, we show that human and murine tumor-infiltrating lymphocytes (TIL) share a core tissue-residency gene-expression signature with Trm. In a mouse model of adoptive T cell therapy for melanoma, Runx3-deficient $CD8^+$ TIL failed to accumulate in tumors, resulting in greater rates of tumor growth and mortality. Conversely, overexpression of Runx3 enhanced TIL abundance, delayed tumor growth, and prolonged survival. In addition to establishing Runx3 as a central regulator of Trm differentiation, these results provide novel insight into the signals that promote T cell residency in tissues, which could be leveraged to enhance vaccine efficacy or adoptive cell therapy treatments that target cancer.

Long-lived memory T cells provide protection from reinfection and can serve as endogenous defenders against tumor growth[3]. Memory $CD8^+$ T cell populations can be broadly segregated into circulating central and effector memory cells (Tcm and Tem) and tissue-resident memory cells (Trm) that primarily reside in non-lymphoid tissues without egress[4]. Circulating memory $CD8^+$ T cells and Trm exhibit distinct gene-expression profiles[5–7]; however, the early transcriptional identity of differentiating Trm and the signals controlling their fate are not yet fully appreciated. Here, we utilized an established infection model where TCR transgenic $CD8^+$ T cells responsive to lymphocytic choriomeningitis virus (LCMV) $GP^{33–41}$ presented by MHC-class $2D^b$ (P14) were transferred into recipient mice followed by infection with LCMV. In this acute infection model, P14 cells located in non-lymphoid tissues on day 7 of infection began to upregulate molecules characteristic of Trm[8], including key tissue-retention molecules CD103 and CD69 (Extended Data Fig. 1a). Gene-expression analysis revealed that 90–96% of the genes upregulated in mature P14 Trm in the kidney parenchyma or intraepithelial lymphocyte (IEL) compartment of the small intestine were elevated in Trm-precursor cells relative to splenic effector cells on day 7 of infection (Fig. 1a). Furthermore, analysis of genes differentially expressed between splenic and non-lymphoid populations on day 7 of infection revealed two distinct gene-expression programs that segregated circulating (PBL, spleen, Tcm, and Tem) from non-lymphoid (kidney and IEL) P14 cells, independent of infection timepoint (Fig. 1b). Lymph node (LN) or splenic $KLRG1^{lo}CD127^{hi}$ memory-precursor (MP) cells preferentially give rise to circulating memory populations whereas shorter-lived $KLRG1^{hi}CD127^{lo}$ terminal effector (TE) cells exhibit less memory potential[3]. Day 7 IEL P14 cells comprising the precursors of Trm, were transcriptionally distinct from splenic MP cells (Fig. 1c). This is notable as IEL Trm are predominantly $KLRG1^{lo}$[,9] and preferentially differentiate from lymphoid-derived $KLRG1^{lo}$ precursors seeding non-lymphoid tissues from days 4.5–7 of infection[10] (Extended Data Fig. 1a–c), consistent with studies of skin Trm[6]. Thus, the Trm-precursor populations in non-lymphoid tissues are transcriptionally distinct from circulating effector cells as well as MP cells on day 7 of infection, and the majority of the Trm transcriptional program is already established at this time point, prior to contraction of the $CD8^+$ T cell population.

As chromatin accessibility is a key determinant of cell identity and fate, we profiled non-lymphoid and splenic effector populations using ATAC-seq on day 7 of infection. Uniquely accessible chromatin regions were identified in IEL P14 cells for genes characteristic of mature Trm (e.g. *Cd69* and *Nr4a1*) whereas genes that promote T cell re-circulation (e.g.

Klf2 and *S1pr1)* exhibited loss of accessible regions (Extended Data Fig. 2a). Principal component analysis (PCA) highlighted that, despite day 7 being an "effector" time point, the global chromatin landscape dramatically differs between effector $CD8^+$ T cells located in the spleen, including MP cells, and those located in non-lymphoid tissues (Fig. 1d). The unique chromatin configuration of differentiating Trm is consistent with the striking transcriptional differences observed (Fig. 1a–c) and foreshadows the distinct fates of antigen-specific cells in the spleen relative to non-lymphoid tissues. Thus, precursors of Trm cells in non-lymphoid sites are a unique and distinct $CD8^+$ T cell subset relative to effector cells in the lymphoid compartment, including the MP population.

Specification of $CD8^+$ T cell fate during infection is dependent on the integrated activity of multiple TFs[3], and notable regulators of Trm formation include Hobit[6], Blimp1[6], Nr4a1[11], Eomes[12], and T-bet[12,13]. To facilitate a broader understanding of the transcriptional network driving Trm differentiation, we utilized a combined screening approach, consisting of a computational strategy integrating ATAC-seq data, transcriptional profiling and personalized PageRank analysis to predict regulatory TFs, and a functional *in vivo* RNAi screen targeting putative Trm regulators identified through the computational approach (Fig. 1e). We recently demonstrated that analysis of accessible TF binding motifs and TF-target gene expression yielded insight into TFs with regulatory functions in the differentiation of circulating memory $CD8^+$ T cells[14]. Leveraging this approach and the personalized PageRank analysis[15], we predicted a number of TFs with established regulatory roles in controlling Trm differentiation (Blimp1[6], Nr4a1[11], Eomes[12], T-bet[12,13]) and many with no previously described role in Trm (Fig. 1f, SI Table 1). We evaluated both barrier (IEL) and non-barrier (kidney) Trm sites to reveal TFs important to Trm differentiation independent of the tissue. Additionally, a key strength of this computational screen is that influential roles of differentially expressed TFs as well as TFs with homogenous expression can be anticipated (Extended Data Fig. 2b). To establish functional relevance for predicted regulators of Trm formation identified through PageRank analysis, we utilized an RNAi screening strategy[16] to test hundreds of individual shRNAmir constructs in parallel for activity in promoting or repressing Trm differentiation *in vivo* (Fig. 1g, SI Table 2). Several TFs with established roles in regulating Trm were identified (Nr4a1[13], Blimp1[6], Klf2[17] and T-bet[12,13]) as well as TFs with previously unknown functions in controlling $CD8^+$ Trm formation such as Nr4a3 and Runx3 (Fig. 1i).

Runx3 is a well-established regulator of $CD8^+$ T cell thymocyte development[18], supports cytotoxic activity of mature $CD8^+$ T cells[19,20], and controls $CD4^+$ T cell localization within the intestinal epithelium[21]. Although little is known regarding a role for Runx3 in $CD8^+$ Trm, both computational and functional screens identified Runx3 as a putative regulator of Trm fate specification (Fig. 1f,g) despite relatively uniform *Runx3* expression in circulating and resident $CD8^+$ T cell subsets (Extended Data Fig. 2b, 3a). We validated a role for Runx3 through a 1:1 mixed transfer of P14 cells transduced with control (*Cd19* shRNAmir) or *Runx3* shRNAmir-encoding retroviruses into mice that were subsequently infected with LCMV (Fig. 2a). *Runx3* shRNAmir suppressed *Runx3* expression (Extended Data Fig. 3b) and impaired the formation of IEL Trm relative to circulating cells (Fig. 2a and Extended Data Fig. 3c,d), consistent with the RNAi screen. Further, *Runx3*-shRNAmir knockdown in

the context of a localized enteric *Listeria monocytogenes* expressing $GP^{33–41}$ (LM-$GP^{33–41}$) infection similarly impaired Trm differentiation (Fig. 2b).

Next, utilizing a tamoxifen-inducible deletion approach, *Runx3*$^{fl/fl}$-Ert2-Cre^{+} P14 (*Runx3*$^{fl/fl}$) or *Runx3*$^{+/+}$-Ert2-Cre^{+} P14 (*Runx3*$^{+/+}$) cells were mixed 1:1 and transferred into host mice followed by LCMV or enteric LM-$GP^{33–41}$ infection (Fig. 2c). *Runx3*-deficiency resulted in a 2–6-fold loss of splenocytes and minimal loss of mLN cells by day 15/16 of infection. However, *Runx3*-deficiency resulted in a 50–150-fold loss of $CD69^{+}CD103^{+}$ Trm in both infection settings (Fig. 2c and Extended Data Fig. 3e). Moreover, delaying tamoxifen treatment to days 6–8 or 16–20 of infection further emphasized a distinct dependence of Trm differentiation on Runx3 (Fig. 2d) as well as a critical role for Runx3 in maintaining Trm homeostasis, respectively (Fig. 2e, Extended Data Fig. 3f). Furthermore, Runx3 was necessary for optimal Trm differentiation of H-$2D^{b}$ $GP^{33–41}$ tetramer^{+} cells (Extended Data Fig. 4a–d). Taken together, these data demonstrate that Runx3 is critical for Trm differentiation and maintenance.

Runx3 deletion also resulted in a loss of Trm in non-barrier tissues (salivary gland and kidney, Extended Data Fig. 5a–b), and optimal Trm differentiation in the skin and lung parenchyma required Runx3 (Extended Data Fig. 5c–h). Thus, the loss of Trm in a range of non-lymphoid tissues indicated Runx3 drives Trm formation independently of the tissue site. Further, Runx3 was required for maximal granzyme B expression in Trm, although cytokine production was not affected (Extended Data Fig. 6a,b). Runx3-deficiency resulted in a greater frequency of Annexin V^{+} cells (Extended Data Fig. 6c,d), most prominently in $CD69^{+}CD103^{+}$ Trm; thus, the marked loss of Trm was at least in part due to a greater rate of apoptosis, as proliferation and trafficking were not impacted (Extended Data Fig. 6e,f).

We next assessed if ectopic expression of Runx3 could augment Trm differentiation. Overexpression of Runx3 accelerated IEL P14 $CD69^{+}CD103^{+}$ Trm differentiation on day 8 of infection, but did not impact migration to the small intestine (Fig. 3a). Evidence of enhanced Trm differentiation was further confirmed by the greater abundance of IEL Trm on day 12/13 of infection and enhanced CD103 expression, consistent with a reported role for Runx3 in regulating CD103 expression[21,22] (Fig. 3b). Additionally, ectopic expression of Runx3 also boosted Trm differentiation in the lung parenchyma (Extended Data Fig. 7a–d).

Given that manipulation of Runx3 impacted Trm formation in diverse tissue microenvironments, we constructed a core Trm transcriptional signature by computational integration of $CD8^{+}$ Trm gene-expression datasets from the IEL, kidney, lung[5], skin[5] and brain[7], to evaluate the hypothesis that *Runx3* is a universal regulator of Trm specification (Fig. 3c, SI Table 3). Notably, we found the majority of the core tissue-residency signature genes were upregulated in Runx3-overexpressing cells and downregulated in *Runx3*-deficient cells. Conversely, the core signature of circulating memory cells was enriched in *Runx3*-deficient cells and depleted from Runx3-overexpressing cells (Fig 3c). Therefore, Runx3 promoted expression of tissue-residency signature genes and repressed genes characteristic of circulating cells, and this conclusion was further corroborated by ChIP-seq analysis[23] indicating that Runx3 binding was enriched in both core tissue-residency and circulating genes relative to background sites (Extended Data Fig. 8a).

Through evaluation of accessible Runx3 binding motifs from ATAC-seq analysis, we generated a regulatory Runx3 binding network (Extended Data Fig. 8b) and found Runx3 putatively regulates a distinct network of genes in differentiating IEL-Trm precursor cells relative to splenic effector cells, including selective enrichment of genes linked to cell adhesion and regulation of TF activity. In connection, Runx3 has been shown to cooperate with the TF T-bet in multiple contexts[19,24], yet T-bet is a potent suppressor of early Trm differentiation[12,13]. ChIP-seq data[23] indicated Runx3 directly binds to multiple sites of the *Tbx21* locus (encoding T-bet, Extended Data Fig. 8c), and *Runx3*-deficient $CD8^+$ T cells exhibited elevated T-bet levels (Extended Data Fig. 8d). Knockdown of *Tbx21* in *Runx3*-deficient cells enhanced Trm numbers in the IEL compartment and restored CD103 and CD69 expression (Extended Data Fig. 8e,f), but did not fully rescue Trm differentiation. These findings are consistent with Runx3 regulating multiple targets that influence Trm formation (Fig. 3c) including suppression of canonical tissue egress genes (Extended Data Fig. 8g,h).

It has been noted that $CD8^+$ tumor infiltrating lymphocytes (TIL) can exhibit characteristics of Trm, and a positive prognosis has been correlated with TIL that present qualities of Trm[25,26]. As Runx3 regulates core features of tissue-residency (Fig. 3c), we assessed the transcriptional similarities of Trm and TIL and evaluated a role for Runx3 in controlling TIL accumulation. TIL isolated from mouse melanoma[27] or mammary tumors[27] shared ~70% of the core tissue-residency gene-expression program relative to splenic $CD8^+$ T cells (Fig. 4a), and this relationship was further highlighted through PCA (Fig. 4b). Utilizing an adoptive therapy model, *Runx3*-knockdown or Runx3-overexpressing P14 cells were mixed with control P14 cells at a 1:1 ratio and transferred into mice with established melanoma tumors expressing $GP^{33–41}$ (Extended Data Fig 9a). *Runx3*-deficiency impaired TIL accumulation (Fig. 4c,d) without impacting migration to the tumor (Extended Data Fig. 9b). Conversely, Runx3-overexpression enhanced TIL abundance (Fig. 4c,d), expression of granzyme B (Extended Data Fig. 9c) and certain core tissue-residency genes while further suppressing core circulating genes (Fig. 4e). In clinical settings, TIL density strongly correlates with positive outcomes[28], and we observed *Runx3*-deficient P14 cells were impaired in their ability to control tumor growth, resulting in greater mortality (Fig. 4f). Conversely, Runx3-overexpressing cells delayed tumor growth and prolonged survival (Fig. 4g). Notably, human $CD8^+$ TIL also exhibited enrichment of the core tissue-residency signature relative to circulating $CD8^+$ T cells[25] (Extended Data Fig. 9d), and analysis of single-cell RNA-seq data from mouse[29] and human melanoma TIL[30] indicated that activated $CD44^+CD8^+$ T cells expressing *Runx3* exhibited enrichment of the tissue-residency gene-expression signature relative to $CD44^+CD8^+$ TIL with low *Runx3* expression levels (Fig. 4h). These data indicate that in both human and murine TIL, tissue-residency features are likely driven by Runx3. In connection, it was recently demonstrated that human lung cancer TIL enriched with certain qualities of Trm also strongly correlated with TIL abundance and a positive prognosis[26]. Taken together, manipulation of TFs promoting tissue-residency may yield more effective TIL and anti-viral memory T cells through supplementing $CD8^+$ T cells with a gene-expression program that better supports features important to both Trm and TIL such as *in situ* survival, tissue retention, and repression of egress, ultimately fostering accumulation of protective T cells in tissues.

Methods

Mice

Mice were maintained in specific-pathogen-free conditions in accordance with the Institutional Animal Care and Use Committees (IACUC) of the University of California, San Diego (UCSD) and The Scripps Research Institute, Jupiter, FL (TSRI-FL). All mice were of a C57BL6/J background and bred at UCSD and TSRI-FL or purchased from the Jackson Laboratory, including: WT or P14 mice with distinct expression of the congenic molecules CD45.1, CD45.2, Thy1.1, and Thy1.2 as well as control Thy1.1^{+}Thy1.2^{+} *Runx3*$^{+/+}$Ert2-Cre^{+}YFP P14 mice and *Runx3* inducible deletion Thy1.1^{+} *Runx3*$^{fl/fl}$Ert2-Cre^{+}YFP P14 mice. *Runx3*$^{+/+}$dLck-Cre^{+}YFP and *Runx3*$^{fl/fl}$dLck-Cre^{+}YFP mice were used for studying polyclonal CD8^{+} T cell responses. The *Rosa26* stop-flox eYFP reporter mice were used for all *Runx3*-deletion experiments. Cre-mediated deletion disrupts the Runx3 DNA-binding domain in exon 4, which exists in transcripts originating from both the distal and proximal promoter. Thus, both long and short Runx3 forms are inactivated in these alleles.

Naive T cell transfers, infection, and treatments

Naive P14 CD8^{+} T cells were transferred intravenously (i.v.) into congenically distinct sex matched recipient mice, or female P14 cells were transferred into male mice. For all microarray, RNA-seq, or ATAC-seq experiments, a total of 1×10^{5} P14 cells were transferred. For co-transfer experiments, naive Thy1.1^{+}Thy1.2^{+} *Runx3*$^{+/+}$ Ert2-Cre YFP^{+} P14 cells and naive Thy1.1^{+} *Runx3*$^{fl/fl}$ Ert2-Cre YFP^{+} P14 cells were mixed 1:1 and a total of 3×10^{4} P14 cells were transferred into Thy1.2^{+} recipient mice. Recipient mice were subsequently infected i.p. with 2×10^{5} PFU of the Armstrong strain of lymphocytic choriomeningitis virus (LCMV) or 10^{10} CFU of Listeria monocytogenes expressing GP$^{33–41}$ via oral gavage[9] one day after cell transfer. For induced *Runx3* deletion, recipient mice were treated with 1mg of tamoxifen diluted in sunflower oil i.p. on days 0–4, 2–5, or 6–8 of infection. For late deletion of Runx3 (days 16–20), recipient mice were treated with 2mg of tamoxifen via oral gavage.

For Trm precursor experiments, 1×10^{5} P14 cells were transferred, recipient mice were infected with LCMV the next day, and KLRG1^{lo} or KLRG1^{hi} P14 cells from spleens and lymph nodes were sorted on day 5 of infection. Sorted cells (1×10^{5}) were transferred into recipient mice infected 4 days prior with LCMV. The number of CD62L^{+} Tcm, CD62L^{-} Tem, or IEL Trm were evaluated on day 20–25 of infection using flow cytometry.

To distinguish vascular associated CD8^{+} T cells in non-lymphoid tissues, 3μg of CD8α (53–6.7) conjugated to APC eFlour780 was injected i.v. into mice four minutes prior to sacrifice and organ excision. CD8α^{neg} cells were considered to be localized within non-lymphoid tissues.

Preparation of cell suspensions

Isolation of CD8^{+} T cells was performed similarly as described[31]. For isolation of CD8^{+} T cells from the small intestine intraepithelial lymphocyte (IEL) compartment, Peyer's patches were removed and the intestine was cut longitudinally and subsequently cut laterally into

0.5–1cm^2 pieces that were then incubated with 0.154mg/mL dithioerythritol (DTE) in 10% HBSS/HEPES bicarbonate for 30min at 37°C while stirring. Kidneys, salivary glands, and lungs were cut into pieces and digested for 30min with 100 U/mL type I collagenase (Worthington) in RPMI 1640, 5% FBS, 2mM $MgCl_2$, 2mM $CaCl_2$ at 37°C while shaking. Skin was processed similarly as described[32] in which a 2cm^2 area of the right flank was excised, pre-digested for 30min at 37°C and then enzymatically digested with 0.7 mg/mL collagenase D. After enzymatic incubations (skin, lungs, kidneys, salivary glands), tissues were further dissociated over a 70μm nylon cell strainer (Falcon). For isolation of lymphocytes, single-cell suspensions were then separated using a 44/67% Percoll density gradient. Spleens and lymph nodes were processed with the frosted ends of microscope slides. Red blood cells were lysed with ACK buffer (140 mM NH_4Cl and 17 mM Tris-base, pH 7.4).

Antibodies, intracellular staining, flow cytometry, and cell sorting

The following antibodies were obtained from eBioscience: CD8α (53–6.7), CD8β (eBio H35–17.2), CD62L (MEL-14), CD127 (A7R34), KLRG1 (2F1), CD103 (2E7), CD69 (H1.2F3), CD45.1 (A20–1.7), CD45.2 (104), Thy1.1 (OX-7, HIS51), Thy1.2 (53–2.1), CCR9 (Ebio CW-1.2), CXCR3 (CXCR3–173), CD49d (R1–2), TNFα (MP6-XT22), GzB (GB11), PD-1 (J43), Tim3 (RMT3–23), Lag3 (eBioC9B7N), KI-67 (SolA15), and IFNγ (XMG1.2) or from BioLegend: CD62L (MEL-14), CD103 (2E7), CD69 (H1.2F3), CD45.1 (A20–1.7), Thy1.1 (OX-7), Thy1.2 (30-H12), and T-bet (4B10). For analysis of apoptosis, the Annexin V Apoptosis Detection Kit was used per manufacturer instructions (eBioscience); propidium iodide negative cells were analyzed for Annexin V staining. The H-2D^b GP$^{33–41}$ tetramer was obtained from the NIH Tetramer Core. For intracellular staining of cytokines or TFs while preserving ametrine or YFP reporter expression in transduced or Cre-YFP$^+$ populations, cells were fixed and permeabilized through a 10min incubation with BD cytofix/cytoperm (BD Biosciences). Intracellular staining was subsequently performed using the Permeabilization Buffer of the Foxp3-Transcription Factor Staining Buffer Set (eBioscience). To assess cytokine production, CD8$^+$ T cells were re-stimulated with the GP$^{33–41}$ peptide in the presence of Protein Transport Inhibitor Cocktail (eBioscience). For flow cytometry analysis, all events were acquired on a BD LSRFortessa X-20 or a BD LSRFortessa. Cell sorting was performed on BD FACSAria or BD FACSAria Fusion instruments.

RNAi screening approach

We have described this screening approach in detail previously[16]. The targeted shRNAmir library was generated based on key genes identified from the computational screening approach as well as genes with known roles in regulating Trm from literature. The library was produced by cloning shERWOOD-designed shRNAmir sequences[33], after PCR of synthetic 97mer oligos, into our pLMPd-Amt vector[16]. Purified DNA from sequence-verified clones was used to package retroviral particles in PLAT-E cells. For transfections, PLAT-E cells were seeded in the middle 60 wells of a 96-well flat bottom plate at a density of 4–6×10^4 cells/well one day prior to transfection. Next, each well was individually transfected with 0.2μg of DNA from each pLMPd-Amt clone and 0.2μg of pCL-Eco using TransIT-LT1 (Mirus). Retroviral supernatant was harvested 36, 48, and 60h after

transfection, and RV sup from each well was used to individually transduce *in vitro* activated P14 cells in 96-well round bottom plates.

For $CD8^+$ T cell activation *in vitro*, naive $CD8^+$ T cells from spleen and lymph nodes were negatively enriched and 2×10^5 P14 cells were plated in the middle 60 wells of 96-well round bottom plates pre-coated with 100μg/mL goat anti-hamster IgG (H+L, Thermoscientific) and 1μg/mL anti-CD3 (145–2C11) and 1μg/mL anti-CD28 (37.51) (both from eBioscience). Culture media was removed 18h after activation, and replaced with retroviral supernatant supplemented with 50μM BME and 8μg/mL polybrene (Millipore) followed by spinfection (60min. centrifugation at 2000 rpm, 37°C). Two hours after the spinfection, the P14 cells were washed 3 times with cold PBS and 90% of each well of cells (individually transduced with distinct retroviral constructs) was harvested, pooled and 5×10^5 pooled P14 cells were transferred into recipient mice which were then infected 1h later with 1.5×10^5 PFU of LCMV clone 13 i.p. 1h later, resulting in an acute infection[16]. The remaining cells *in vitro* were cultured for an additional 24h and either pooled for “input” sequencing (6×10^5 P14 cells) or were used to test transduction efficiency of each construct using flow cytometry to detect the percentage of ametrine$^+$ cells in each well.

Twelve days after infection, spleens and small intestines were harvested from 15–18 mice and splenocytes and IEL P14 cells were processed as described above. Prior to sorting, all IEL or splenic samples were pooled. $CD62L^+$ P14 cells (Tcm) from the spleen as well as P14 cells from the IEL were sorted ($2–6\times10^5$ cells total). Genomic DNA was then harvested from sorted cells using the FlexiGene kit (Qiagen). The integrated proviral passenger strand shRNAmir sequences in each cell subset were amplified from 20–100ng total genomic DNA per reaction, with 23–28 cycles of PCR using Ion Proton-compatible barcoded primers that anneal to the common 5′ mir30 and shRNAmir loop sequences. 2–3 replicate reactions were performed for each genomic DNA sample and the replicates were pooled after amplification. The pooled reactions were purified using AMPure XP beads, the amplicons in each sample were quantified using a Bioanalyzer, and then pooled in a 1:1 molar ratio for sequencing. In each replicate of the screen, a minimum of 2.5 million reads per sample were generated and retained, after filtering low-quality reads. Reads assigned to each barcode were aligned to a reference database of all shRNAmirs in the library using BLAST and a custom script to count the top alignment of each read and summarize the number of reads aligned to each shRNAmir.

For analysis of shRNAmir representation in Tcm relative to IEL Trm, the total number of reads in each of the samples was normalized, and the number of reads for each shRNAmir was scaled proportionally. Subsequently, the normalized number of reads in the IEL Trm cells for a given shRNAmir was divided by the normalized number of reads for the same shRNAmir in the Tcm sample and then $\log_2$ transformed. The mean and standard deviation of the ratios of each of the 25 negative control shRNAmir constructs (targeting *Cd19, Cd4, Cd14, Ms4a1, Cd22, Hes1, Klf12, Mafb, Plagl1, Pou2af1*, and *Smarca1*) were used to calculate the Z-score for each shRNAmir construct. The screen was repeated three times and the Z-score of each construct from each individual screen was averaged and plotted (Fig. 1i, SI Table 2). Certain constructs were added after the first screen or were not detectable in one of the screens, but all constructs were successfully screened 2–3 times except for 13

constructs, which are marked by an asterisk in SI Table 2. Eighty-four percent (21/25) of all negative control shRNAmir constructs had an average Z-score between −0.9 and 0.9.

CD8$^+$ T cell transduction, cell transfer, and infection for individual analysis of retroviral constructs

Activation, transfections, and transductions were carried out as described for the RNAi screening approach except in some experiments 2×10^6 P14 cells were activated per well in 6-well plates. Congenically distinct P14 cells transduced with the *Runx3.2* shRNAmir or *Cd19.1* shRNAmir (control) retroviruses were mixed 1:1 within 24h of transduction and a total of $1–5\times10^5$ P14 cells were transferred i.v. into recipient mice. One hour after adoptive transfer, recipient mice were infected i.p. or intratracheally (i.t.) with 2×10^5 PFU LCMV armstrong or intradermally (i.d.) with 2×10^4 PFU clone 13. In similar experiments, P14 cells were transduced with MigR1-based retroviruses[34] that were empty (GFP-RV) or that contained Runx3 cDNA (Runx3-RV), mixed 1:1 and transferred to recipient mice for subsequent infections. For T-bet rescue experiments, Thy1.2$^+$ *Runx3*$^{+/+}$ Ert2-Cre YFP$^+$ P14 cells were transduced with *Cd19.1* shRNAmir and Thy1.1$^+$ *Runx3*$^{fl/fl}$ Ert2-Cre YFP$^+$ P14 cells were transduced with *Tbx21.3* shRNAmir, mixed 1:1 and transferred into recipient mice, which were infected 1h later with LCMV armstrong i.p. and treated with 1mg tamoxifen i.p. for five consecutive days starting with the day of infection.

Adoptive therapy tumor model

For adoptive therapy experiments, 5×10^5 B16-GP^{33} cells, treated for mycoplasma contamination and authenticated in *in vitro* killing assays, were transplanted subcutaneously into the right flank of wild-type mice. After tumors became palpable, 7–8 days post-transplant, *in vitro* expanded P14 cells were transferred i.v. For comparison of TIL accumulation in a mixed transfer setting, naive P14 cells were activated, transduced, and expanded with 100U/mL of IL-2 for 2–3 days; cells transduced with control constructs (*Cd19.1* shRNAmir or GFP-RV) or experimental constructs (*Runx3.2* shRNAmir or Runx3-RV) were mixed 1:1 and $0.5–1\times10^6$ P14 cells were transferred i.v. For efficacy studies, transduced cells were expanded for 5–6 days; transduced cells were then sorted (or not sorted with a Runx3-RV and GFP-RV transduction efficiency >83%), and $1–2.5\times10^6$ cells were transferred i.v. into mice with established B16-GP^{33} tumors. Tumors were monitored daily and mice with ulcerated tumors or tumors exceeding 1500 mm^3 were euthanized, in accordance with UCSD IACUC .

qPCR, Microarray, RNA-seq, and ATAC-seq analysis

For validation of the Runx3-RV overexpression construct and *Runx3.2* shRNAmir construct, enriched CD8$^+$ T cells were activated, transduced, and expanded for 4–6 days in 100U/mL IL-2. Cells were sorted on ametrine (*Runx3* shRNAmir or Con shRNAmir) or GFP (Runx3-RV or GFP-RV) directly into TRIzol (Life Technologies) and RNA was extracted per manufacturer's specifications. Next, cDNA was synthesized using Superscript II (Life Technologies) and qPCR was performed using the Stratagene Brilliant II Syber Green master mix (Agilent Technologies). *Runx3* expression levels were normalized to the housekeeping gene *Hprt*. We have previously validated the *Tbx21.3* shRNAmir[16]. The following primers were used for qPCR: *Runx3* forward, 5′-

CAGGTTCAACGACCTTCGATT-3′, and *Runx3* reverse, 5′-GTGGTAGGTAGCCACTTGGG-3′; *Hprt* forward, 5′-GGCCAGACTTTGTTGGATTT-3′, and *Hprt* reverse, 5′-CAACTTGCGCTCATCTTAGG-3′.

On day 7 of infection, tissues from 2–3 mice were pooled and 2–3×10^4 P14 cells from the IEL, kidney, spleen, or blood were sorted into TRIzol. On day 35 of infection, tissues from 5–10 mice were pooled and 1–2×10^4 CD62L$^+$ Tcm, CD62L$^-$ Tem, kidney Trm, and IEL Trm P14 cells were sorted into TRIzol. As described previously, RNA was amplified and labeled with biotin and hybridized to Affymetrix Mouse Gene ST 1.0 micrroarrays (Affymetrix)[35]. Analyses were performed using GenePattern Multiplot Studio. Differentially expressed genes in IEL Trm compared to Tcm and Tem as well as kidney Trm compared to Tcm and Tem were identified with a fold change (FC) >1.5 and an expression value (EV) >120 (Fig. 1a). Genes with >1.5 FC and >120 EV between day 7 spleen, day 7 IEL, and day 7 kidney samples were identified (1838 probes) and evaluated in day 7 and day 35 subsets, which were ordered with Pearson correlation using the HierarchicalClustering module of GenePattern (Fig. 1b); data was row centered, row normalized, and visualized with the HierarchicalClusteringViewer module within GenePattern.

The core Trm and circulating signatures were generated by integrating differential expression (>1.5 FC) data comparing Trm from the following tissues to circulating splenic memory cells (or splenic Tcm if both Tcm and Tem datasets were available): D35 IEL (LCMV), D35 kidney parenchyma (LCMV), D30 skin CD103$^+$CD8$^+$ (herpes simplex virus)[5], D30 lung CD103$^+$CD8$^+$ (influenza virus)[5], and D20 CD103$^+$ brain (vesicular stomatitis virus)[7]; overlapping genes upregulated in all Trm populations comprised the core tissue-residency signature (121 genes) and genes downregulated in all populations comprised the circulating signature (93 genes). The mouse TIL microarray datasets were generated previously[27].

For RNA-seq analysis of D7 IEL, D7 MP, and D7 TE, the populations were sorted on day 7 of LCMV Armstrong infection as well as naive P14 cells; spleens or IEL samples from 2–3 mice were pooled and 5×10^3 cells were sorted. For RNA-seq analysis of TIL, congenically distinct P14 cells were transduced with Runx3-RV or GFP-RV, mixed 1:1 and 1×10^6 were transferred to mice with day 7 established melanoma B16-GP[33] tumors. Eight days later, 1×10^3 transduced TIL or splenocytes were sorted from 4 mice for each replicate. For library preparation, isolation of polyA$^+$ RNA was performed as detailed online (www.immgen.com/Protocols/11cells.pdf). For RNA-seq analyses of *Runx3*-manipulated cells, CD8$^+$ T cells from naive *Runx3*$^{+/+}$ YFP$^+$ (WT) and *Runx3*$^{fl/fl}$ YFP$^+$ (*Runx3*$^{fl/fl}$) mice were enriched by negative isolation and transduced (as detailed above) with a Cre cDNA expressing retrovirus (Cre-RV). *Runx3*-overexpressing cells were generated similarly by transducing *Runx3*$^{+/+}$ YFP$^+$ CD8 T cells with a Runx3-cDNA expressing retrovirus (Runx3-RV). Forty-eight hours after TCR activation, the CD8$^+$ T cells were resuspended and re-cultured in fresh media supplemented with 100U/mL rhIL-2; twenty-four hours later, YFP$^+$ ("WT" or "*Runx3*$^{fl/fl}$") or GFP$^+$ (Runx3-RV) were FACS-purified and then recultured in 100U/mL IL-2. The cells were expanded until day 6 by reculturing at 5×10^5 cells/mL every 24h in fresh 100U/mL IL-2 media. On day 6 post-activation, cells were harvested and total RNA was extracted in TRIzol. Purified RNA was depleted of ribosomal RNA and strand-specific

paired-end libraries were prepared and sequenced using an Illumina Nextseq 500. Samples were generated from two biological replicates, and approximately 20 million paired-reads were generated per sample. Reads were mapped using Tophat[36] and aligned reads in transcripts were counted with HTseq[37]. Gene-set-enrichment analysis (GSEA) was performed by using the GSEA module in GenePattern, and the normalized enrichment scores and false-discovery rate q values were determined by using the permutation test.

ATAC-seq was performed as described in detail previously[24]. Sorted cells (2.5×10^4) were resuspended in 25μL of lysis buffer and spun down 600*g* for 30min at 4°C. The nuclear pellet was resuspended in 25μL of Tn5 transposase reaction mixture (Nextera DNA Sample Prep Kit, Illumina) and incubated for 30min at 37°C. Transposase-associated DNA was subsequently purified (Zymo DNA clean-up kit). For library amplification, DNA was amplified using indexing primer from Nextera kit and NEBNext High-Fidelity 2X PCR master mix. Then, the amplified DNA was size-selected to fragments less than 800 bp using SPRI beads. The library was sequenced using Hiseq 2500 for single-end 50-bp sequencing to yield at least 10 million reads. We used bowtie to map raw reads to the *Mus musculus* genome (mm10) with following parameters: "–best -m 1". We called peaks for each individual replicate as well as the pooled data from the two replicates using MACS2 with a relaxed threshold (*P*-value 0.01).

For the single cell RNA-seq analysis of human[30] and mouse melanoma TIL[29], the preprocessed single cell TIL gene expression data was downloaded from GEO database GSE72056 or GSE86042, respectively. Activated $CD8^+$ TIL (CD8a expression >5 and CD44 expression>2) was used and classified into *Runx3*^{hi} TIL, which express relatively high levels of *Runx3* (*Runx3* expression>3) and *Runx3*^{lo} TIL with no *Runx3* expression (*Runx3* expression=0). For the human TIL, melanoma #75 was used. GSEA was performed to evaluate enrichment of the core tissue-residency gene expression signature in *Runx3*^{hi} TIL relative to *Runx3*^{lo} TIL.

Computational Screen: TF regulatory networks and personalized PageRank analysis

TF regulatory networks and PageRank analysis was performed similarly as described[24] except that gene expression and ATAC-seq data from D7 IEL, D7 kidney and D7 spleen samples were used. To construct the TF regulatory network, TF-binding motifs were first scanned on ATAC-seq peaks using an algorithm described previously[14] and a P-value cutoff of 1×10^{-5}. Then, we connected a TF to a gene if the TF had any predicted binding motif in the ATAC-seq peak of the nearest gene. We assembled all the interactions between TFs and genes into a regulatory network. To identify important TF regulators for Trm differentiation, we performed personalized PageRank analysis in the TF regulatory network constructed above using the pipeline described previously[14]. The importance of a TF is based on the quantity and quality of its regulated gene targets. A TF would receive a higher PageRank score if it regulates more important genes where the importance is evaluated by differential expression from microarray or RNA-seq analyses. Extended Data Fig. 2b and SI Table 1 indicate the PageRank score and expression value of all TFs expressed (>120 EV) in the spleen, kidney or IEL cells.

Statistical analysis

Student's t-test (two-tailed) was used for comparisons between two groups. Log-rank (Mantel-Cox) test was used to compare survival curves. All microarray, RNAseq, and ATACseq samples were performed independently in 2–3 replicates. All statistical tests were performed with GraphPad Prism software and P<0.05 was considered statistically significant.

Data Availability

RNA-seq, microarray, and ATAC-seq data are available in the GEO database: accession codes (will be provided). Source Data are provided in the online version of the manuscript. Additional information and materials will be made available upon request.

Extended Data

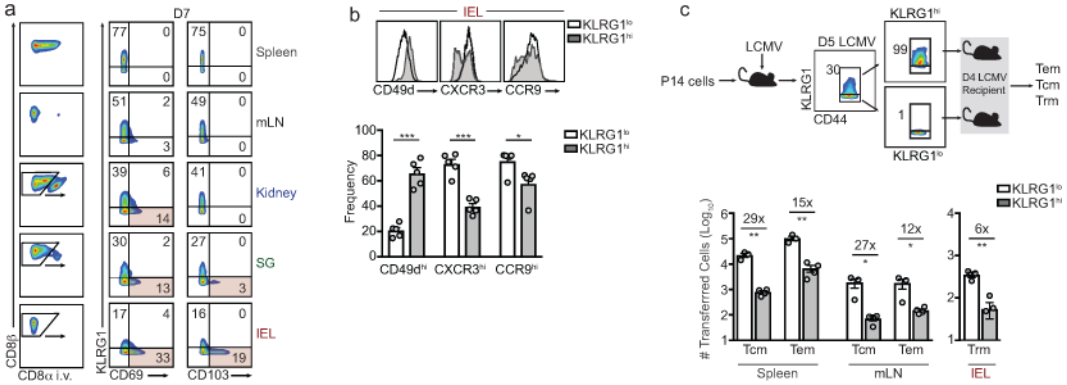

Extended Data Figure 1. KLRG1^{lo} cells preferentially give rise to Trm

a, Representative flow cytometric gating strategy for distinguishing P14 cells located in non-lymphoid tissues following CD8α i.v. administration in LCMV infected mice (left). Right, *in vitro* activated P14 cells were transferred to recipient mice and infected with LCMV and the frequency of CD69^{+} and CD103^{+} P14 cells among KLRG1^{hi} and KLRG1^{lo} on day 7 of infection is indicated. **b**, Frequency of CCR9, CXCR3, and CD49d on KLRG1^{lo} and KLRG1^{hi} cells in the IEL compartment on day 7 of infection. **c**, Schematic of experimental design (top). KLRG1^{lo} and KLRG1^{hi} P14 cells were sorted from spleens and LNs on day 5 of LCMV infection and transferred into recipient mice infected 4 days prior with LCMV. Tcm, Tem, and Trm P14 cells were enumerated on days 20 or 25 of infection using flow cytometry (bottom). Graphs indicate mean ± s.e.m of n=5 mice (**a,b**) or n=3–4 mice (**c**) from one representative of 2 independent experiments, *P<0.05, **P<0.01, ***P<0.005. Symbols represent an individual mouse (**c**).

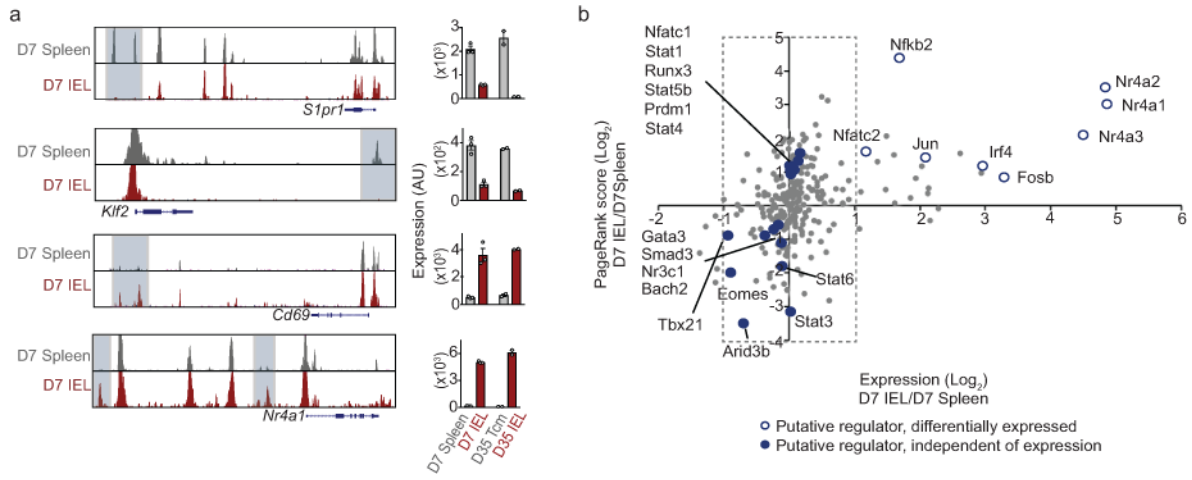

Extended Data Figure 2. Representative ATAC-seq peaks and putative Trm regulators identified through PageRank analysis

a, ATAC-seq analysis of the indicated loci on day 7 of infection (left) and corresponding gene expression (right). **b**, Personalized PageRank score and gene-expression of TFs with select TFs highlighted.

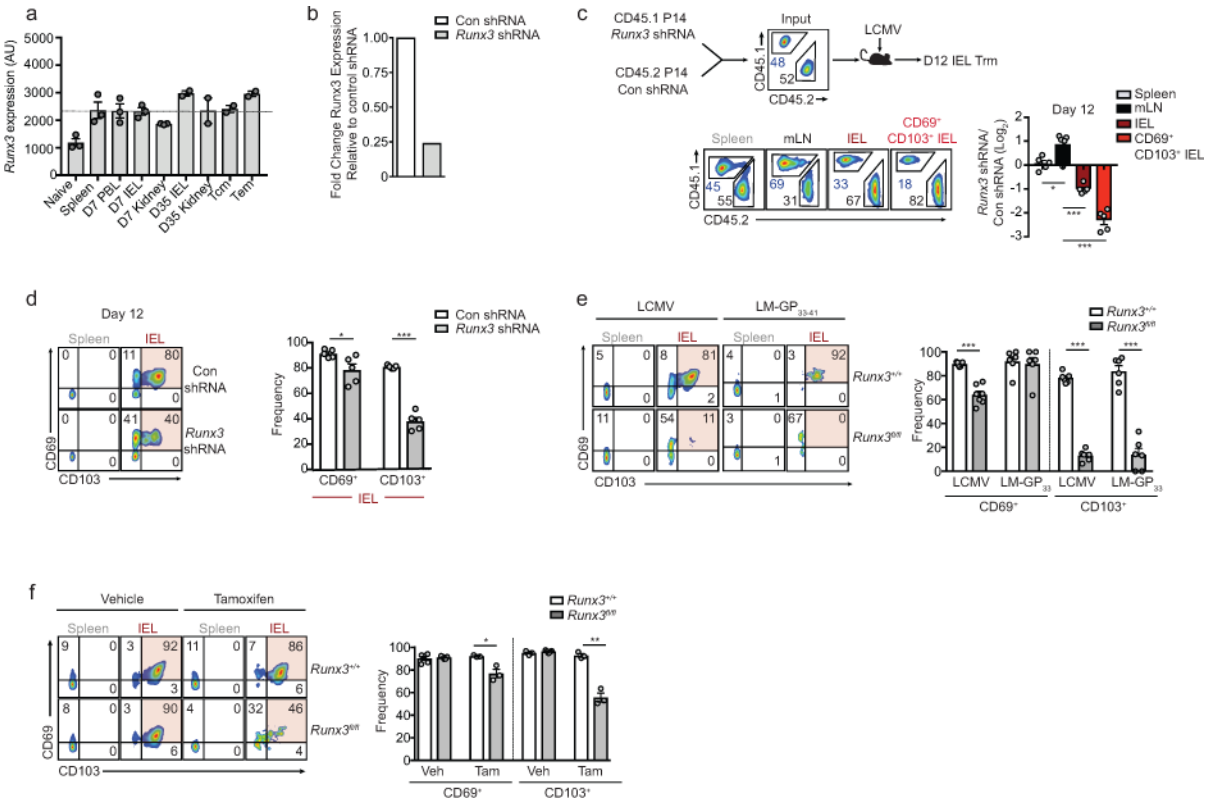

Extended Data Figure 3. Runx3-deficiency impairs IEL Trm formation

a, *Runx3* mRNA levels from indicated cells determined by microarray analyses. **b**, Relative *Runx3* mRNA expression of *in vitro* cultured cells transduced with Con shRNAmir or *Runx3* shRNAmir-encoding retroviruses measured by qPCR. **c**, Congenically distinct P14

cells were transduced with *Runx3* shRNAmir or Con shRNAmir encoding retroviruses, mixed at a 1:1 ratio, and transferred to recipient mice that were subsequently infected with LCMV. Representative flow cytometry plots (bottom, left) and quantification of the ratio of *Runx3* shRNAmir or control shRNAmir transduced P14 cells in indicated tissues on day 12 of infection (bottom, right). **d**, Representative flow cytometry plots (left) and quantification of the frequency of $CD69^+$ and $CD103^+$ cells of Con shRNAmir or *Runx3* shRNAmir cells (right) from experimental schematic in **c**. **e**, Representative flow cytometry plots and quantification of the frequency of $CD69^+$ and $CD103^+$ cells from Fig. 2 c,d. **f**, Representative flow cytometry plots and quantification of the frequency of $CD69^+$ and $CD103^+$ cells from Fig. 2f. Graphs indicate mean ± s.e.m and representative of two independent experiments (**b**) with n=5 (**c**,**d**), n=5 (LM-$GP^{33–41}$) or n=6 (LCMV) (**e**), and n=5 (vehicle) or n=3 (tamoxifen) (**f**), *P<0.05, **P<0.01 ***P<0.005. Symbols represent an individual mouse (**c–f**).

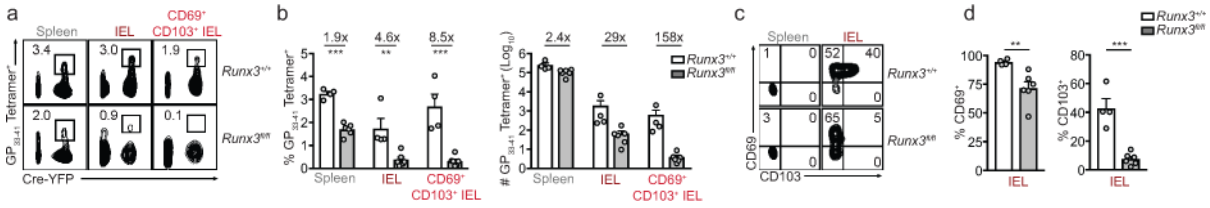

Extended Data Figure 4. Runx3-deficiency impairs IEL Trm formation in a polyclonal setting

a, Representative flow cytometry plot of H-$2D^b$ $GP^{33–41}$ tetramer staining of lymphocytes from $Runx3^{fl/fl}$ dLck-Cre^+YFP and $Runx3^{+/+}$dLck-Cre^+YFP mice on day 12 of LCMV infection (gated on total lymphocytes). **b**, Quantification of the proportion (left) and absolute number (right) of $tetramer^+$ cells. **c**,**d**, Representative flow cytometry plots and quantification of the frequency of $CD69^+$ and $CD103^+$ cells. Graphs indicate mean ± s.e.m with n=4 (*$Runx3^{+/+}$*) or n=5 (*$Runx3^{fl/fl}$*) mice pooled from two independent experiments, **P<0.01, ***P<0.005. Symbols represent an individual mouse (**b,d**).

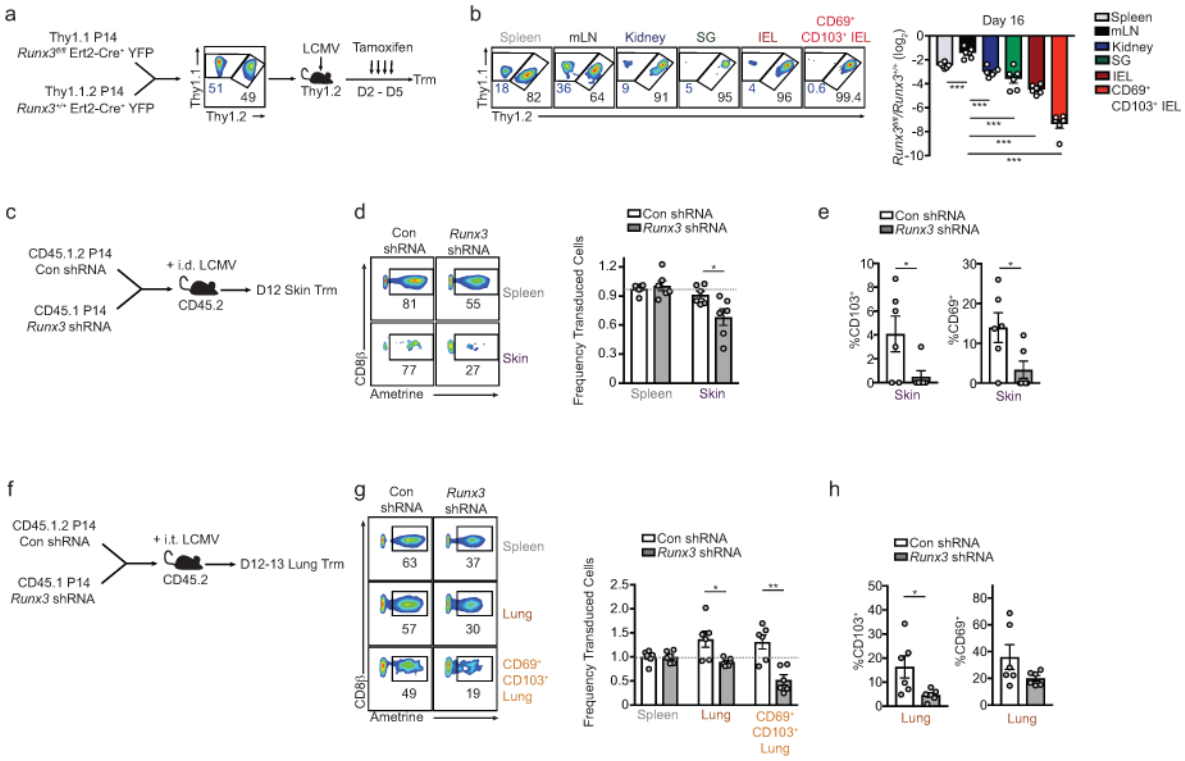

Extended Data Figure 5. Runx3 is required for Trm formation in diverse non-lymphoid tissues

a, Schematic of experimental design. **b**, Representative flow cytometry plots (left) and quantification (right) of the ratio *Runx3*$^{fl/fl}$ and *Runx3*$^{+/+}$ P14 cells (gated on YFP-Cre^{+} cells) in lymphoid and non-lymphoid compartments on days 15/16 of LCMV infection (same data as in Fig. 2d but including SG and kidney populations). **c**, Schematic for experimental design. **d**, Representative flow cytometry plots (left) and quantification (right) of the ratio of transduced cells in the skin relative to the spleen for Con shRNAmir or *Runx3* shRNAmir P14 cells on day 12 of an intradermal (i.d.) LCMV infection. **e**, Frequency of CD69^{+} and CD103^{+} cells. **f**, Schematic for experimental design. **g**, Representative flow cytometry plots (left) and quantification (right) of the ratio of transduced cells in the lung parenchyma relative to the spleen for Con shRNAmir or *Runx3* shRNAmir P14 cells on day 12 of an intratracheal (i.t.) LCMV infection. **h**, Frequency of CD69^{+} and CD103^{+} cells. Graphs indicate mean ± s.e.m and representative of two independent experiments with n=6 (**b**), or data pooled from two individual experiments with n=6 per group (**c–h**), *P<0.05, **P<0.01, ***P<0.005. Symbols represent an individual mouse (**b**,**d**,**e**,**g**,**h**).

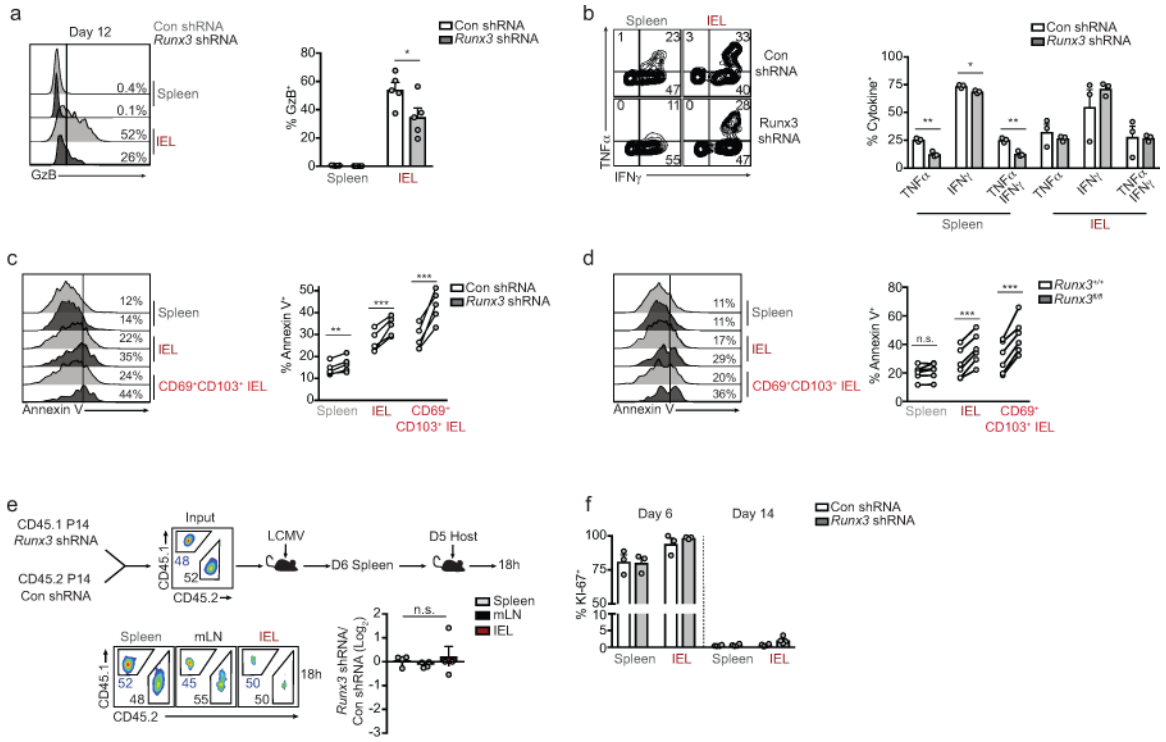

Extended Data Figure 6. Runx3-deficiency enhances Trm apoptosis but does impact trafficking or proliferation

a, Representative flow cytometry histogram of granzyme B (GzB) staining (left) and quantification of frequency of GzB^+ cells on day 12 or 14 of infection. **b**, Representative flow cytometry plots (left) and quantification (right) of the frequency of IFNγ- and TNFα-producing Con shRNAmir or *Runx3* shRNAmir P14 cells on day 6 of LCMV infection, restimulated with $GP^{33–41}$ peptide. **c**,**d**, Representative histograms and quantification of Annexin V^+ cells from shRNAmir mixed transfers on day 14 of LCMV infection (**c**) or from day 8 $Runx3^{fl/fl}$ and $Runx3^{+/+}$ mixed P14 transfers where tamoxifen was administered on days 2–5 of LCMV infection (**d**). **e**, Congenically distinct P14 cells were transduced with Con shRNAmir or *Runx3* shRNAmir encoding retroviruses, mixed at a 1:1 ratio, and transferred to recipient mice that were subsequently infected with LCMV. On day 6 of infection, splenocytes were harvested and retransferred to day 5 infected host mice and 18h later spleen, mLN and small intestine were harvested to assess trafficking. Representative flow cytometry plots (bottom, left) and quantification of the ratio of Con shRNAmir and *Runx3* shRNAmir transduced P14 cells (bottom, right) in indicated tissues 18h after transfer. **f**, Frequency of KI-67^+ Con shRNAmir or *Runx3* shRNAmir transduced P14 cells in a mixed transfer setting on days 6 and 12 or 14 of LCMV infection. Graphs indicate mean ± s.e.m and representative of two independent experiments with n=5 (**a**), n=3 (**b**), n=5 (**c**), n=6 (**d**), n=4 (**e**), and n=3 on day 6 or n=4 on day 14 (**f**) except **d** is pooled from two independent experiments, *P<0.05, **P<0.01, ***P<0.005, n.s., not significant. Symbols represent an individual mouse (**a–f**).

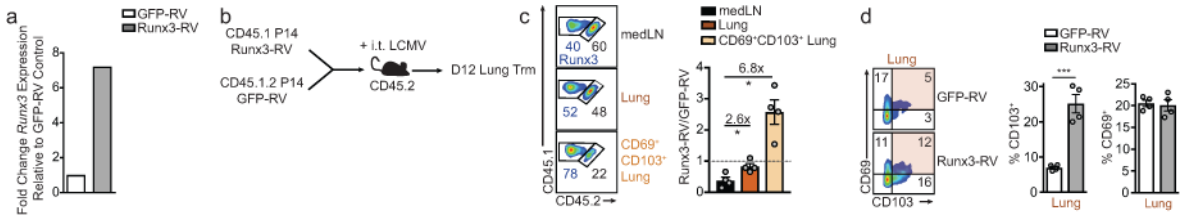

Extended Data Figure 7. Runx3 overexpression enhances lung Trm differentiation

a, *Runx3* mRNA expression of *in vitro* cultured cells transduced with GFP-RV or Runx3-RV. **b**, Schematic for experimental design of intratracheal (i.t.) LCMV infection. **c**, Representative flow cytometry plots (left) and quantification (right) of the ratio of GFP-RV or Runx3-RV cells in the mediastinal LN (medLN), lung parenchyma, or CD69^{+}CD103^{+} lung parenchyma population on day 12 or 13. **d**, Representative flow cytometry plots (left) and quantification (right) of the frequency of CD69^{+} and CD103^{+} P14 cells in the lung parenchyma. Graphs indicate mean ± s.e.m and data representative of one of two independent experiments (**a**) and n=4 per group (**c**,**d**), *P<0.05, ***P<0.005. Symbols represent an individual mouse (**c**,**d**).

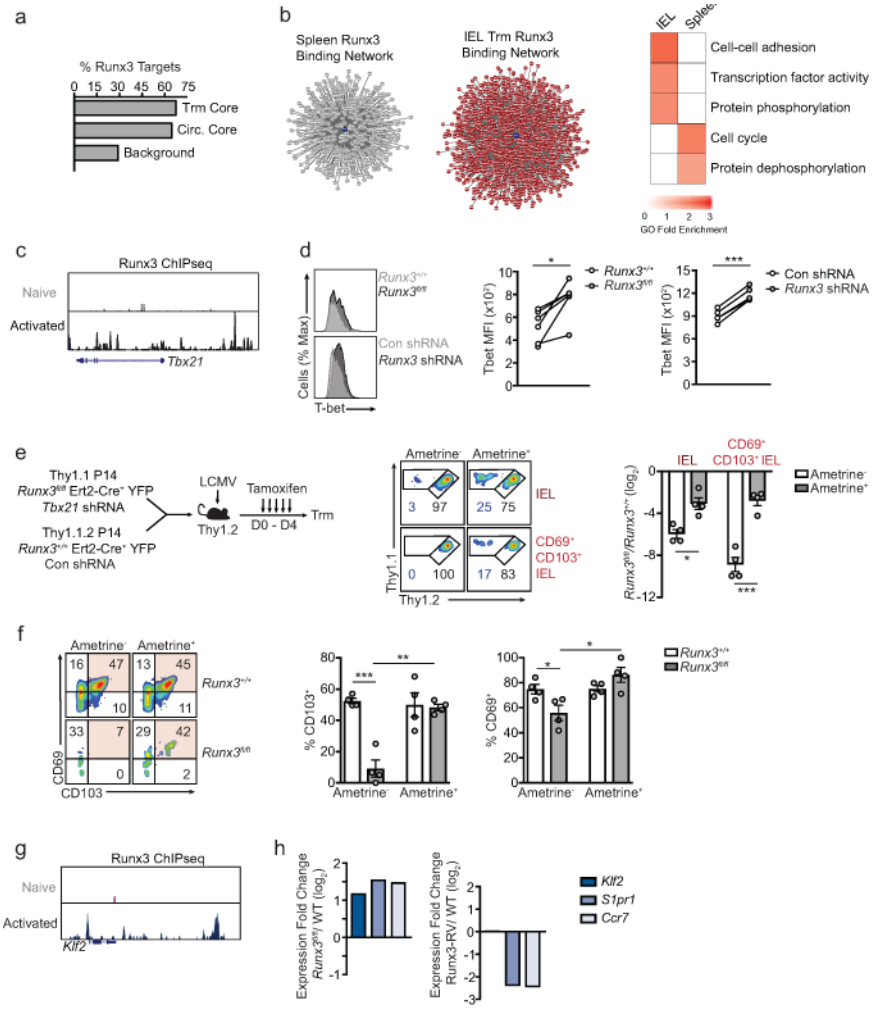

Extended Data Figure 8. Runx3 regulates distinct gene programs in circulating cells versus tissue resident cells and operates upstream of T-bet in programming IEL Trm differentiation

a, Percentage of genes of the core tissue-residency signature, core circulating signature, or background sites that exhibit direct Runx3 binding by ChIP-seq analysis[23]. **b**, Predicted Runx3 binding network, generated from ATAC-seq analysis, in IEL P14 cells and splenic P14 cells on day 7 of infection (left). Red indicates genes putatively regulated by Runx3 in IEL cells; grey indicates genes putatively regulated by Runx3 in splenic cells. Gene Ontology (GO) enrichment analysis (right) of gene sets in the predicted Runx3 binding network in each tissue. **c**, Runx3 ChIP-seq of the *Tbx21* locus in naive and activated $CD8^+$ T cells from Lotem et al.[23]. **d**, Representative flow cytometry histograms (left) and MFI quantification (right) of T-bet expression in splenic P14 cells on day 8 of infection. **e**, Schematic for experimental design (left) in which *Runx3*$^{+/+}$Ert2-Cre^+YFP were transduced with Con shRNAmir and *Runx3*$^{+/+}$Ert2-Cre^+YFP P14 cells were transduced with *Tbx21* shRNAmir, mixed 1:1 and transferred into recipient mice subsequently infected with LCMV. Recipient mice were treated with tamoxifen on days 0–4 of infection. Representative flow cytometry plots (middle panel) and quantification of the ratio of untransduced (ametrine$^-$) *Runx3*$^{+/+}$ and *Runx3*$^{fl/fl}$ P14 cells and the ratio of transduced (ametrine$^+$) *Runx3*$^{+/+}$/Con shRNAmir and *Runx3*$^{fl/fl}$/*Tbx21* shRNAmir (right) were evaluated on day 12 of LCMV infection. **f**, Representative flow cytometry plots (left) and quantification (right) of the frequency of $CD69^+$ and $CD103^+$ cells. **g**, Runx3 ChIPseq of the *Klf2* locus in naive and activated $CD8^+$ T cells[23]. **h**, Fold change in gene-expression of *Klf2*, *S1pr1*, and *Ccr7* in Runx3$^{fl/fl}$ and Runx3-RV cells relative to Runx3$^{+/+}$ WT cells, from RNA-seq analysis consisting of 2 replicates per sample. Graphs indicate mean ± s.e.m and data representative of one of two independent experiments with n=6 (*Runx3*$^{fl/fl}$) or n=4 (*Runx3* shRNA) (**d**) and n=4 per group(**e**,**f**). *P<0.05, **P<0.01 ***P<0.005. Symbols represent an individual mouse (**d–f**).

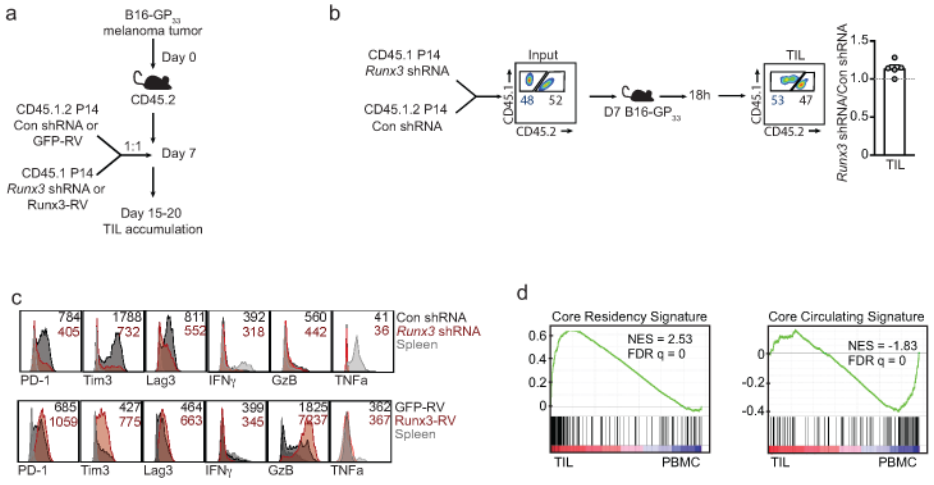

Extended Data Figure 9. *Runx3*-deficiency does not impair trafficking to the tumor but impacts the effector phenotype of TIL

a, Schematic of adoptive therapy experimental design. **b**, Congenically distinct P14 cells were transduced with *Runx3* shRNAmir or Con shRNAmir encoding retroviruses, mixed at a 1:1 ratio, and transferred into mice with established B16-GP^{33} melanoma tumors. Eighteen

hours after transfer, tumors were harvested to assess the ratio of *Runx3* shRNAmir or Con shRNAmir P14 cells. **c**, Representative flow cytometry histograms of Con shRNAmir, *Runx3* shRNAmir, GFP-RV, or Runx3-RV TIL in mixed transfer settings. Control P14 splenocytes were included in histograms for reference. **d**, Gene set enrichment analysis of the core tissue-residency and core circulating gene signatures in human lung $CD8^+$ TIL relative to corresponding $CD8^+$ PBMCs[25]. Graphs indicate mean ± s.e.m and combined of two independent experiments with n=5 mice per group (**b**) or representative of two independent experiments with n=3–6 per group (**b**). Symbols represent an individual mouse (**b**).

Supplementary Material

Refer to Web version on PubMed Central for supplementary material.

Acknowledgments

We thank all the members of the Goldrath and Pipkin laboratories for their contributions. We also thank the Flow Cytometry Core at the La Jolla Institute for Allergy and Immunology. This study was funded in part by the US National Institutes of Health U19AI109976 (S.C., M.E.P., A.W.G), California Institute for Regenerative Medicine RB5-07012 (W.W.).

References

1. Jiang X, et al. Skin infection generates non-migratory memory CD8+ T(RM) cells providing global skin immunity. Nature. 2012; 483:227–231. [PubMed: 22388819]
2. Schenkel JM, et al. Resident memory CD8 T cells trigger protective innate and adaptive immune responses. Science. 2014; 346:98–101. [PubMed: 25170049]
3. Chang JT, Wherry EJ, Goldrath AW. Molecular regulation of effector and memory T cell differentiation. Nat Immunol. 2014; 15:1104–1115. [PubMed: 25396352]
4. Mueller SN, Gebhardt T, Carbone FR, Heath WR. Memory T cell subsets, migration patterns, and tissue residence. Annu Rev Immunol. 2013; 31:137–161. [PubMed: 23215646]
5. Mackay LK, et al. The developmental pathway for CD103+ CD8+ tissue-resident memory T cells of skin. Nat Immunol. 2013; 14:1294–1301. [PubMed: 24162776]
6. Mackay LK, et al. Hobit and Blimp1 instruct a universal transcriptional program of tissue residency in lymphocytes. Science. 2016; 352:459–463. [PubMed: 27102484]
7. Wakim LM, et al. The molecular signature of tissue resident memory CD8 T cells isolated from the brain. J Immunol. 2012; 189:3462–3471. [PubMed: 22922816]
8. Masopust D, Vezys V, Wherry EJ, Barber DL, Ahmed R. Cutting edge: gut microenvironment promotes differentiation of a unique memory CD8 T cell population. J Immunol. 2006; 176:2079–2083. [PubMed: 16455963]
9. Sheridan BS, et al. Oral infection drives a distinct population of intestinal resident memory CD8+ T cells with enhanced protective function. Immunity. 2014; 40:747–757. [PubMed: 24792910]
10. Masopust D, et al. Dynamic T cell migration program provides resident memory within intestinal epithelium. J Exp Med. 2010; 207:553–564. [PubMed: 20156972]
11. Boddupalli CS, et al. ABC transporters and NR4A1 identify a quiescent subset of tissue-resident memory T cells. J Clin Invest. 2016; 126:3905–3916. [PubMed: 27617863]
12. Mackay LK, et al. T-box Transcription Factors Combine with the Cytokines TGF-β and IL-15 to Control Tissue-Resident Memory T Cell Fate. Immunity. 2015; 43:1101–1111. [PubMed: 26682984]
13. Laidlaw BJ, et al. CD4+ T cell help guides formation of CD103+ lung-resident memory CD8+ T cells during influenza viral infection. Immunity. 2014; 41:633–645. [PubMed: 25308332]

14. Yu B, et al. Epigenetic landscapes reveal transcription factors that regulate CD8+ T cell differentiation. Nat Immunol. 2017
15. Page L, Brin S, Motwani R, Winograd T. The PageRank citation ranking: Bringing order to the web. World Wide Web (Bussum). 1998; 54:1–17.
16. Chen R, et al. In vivo RNA interference screens identify regulators of antiviral CD4+ and CD8+ T cell differentiation. Immunity. 2014; 41:325–338. [PubMed: 25148027]
17. Skon CN, et al. Transcriptional downregulation of S1pr1 is required for the establishment of resident memory CD8+ T cells. Nat Immunol. 2013; 14:1285–1293. [PubMed: 24162775]
18. Taniuchi I, et al. Differential requirements for Runx proteins in CD4 repression and epigenetic silencing during T lymphocyte development. Cell. 2002; 111:621–633. [PubMed: 12464175]
19. Cruz-Guilloty F, et al. Runx3 and T-box proteins cooperate to establish the transcriptional program of effector CTLs. J Exp Med. 2009; 206:51–59. [PubMed: 19139168]
20. Shan Q, et al. The transcription factor Runx3 guards cytotoxic CD8+ effector T cells against deviation towards follicular helper T cell lineage. Nat Immunol. 2017; 18:931–939. [PubMed: 28604718]
21. Reis BS, Rogoz A, Costa-Pinto FA, Taniuchi I, Mucida D. Mutual expression of the transcription factors Runx3 and ThPOK regulates intestinal CD4+ T cell immunity. Nat Immunol. 2013; 14:271–280. [PubMed: 23334789]
22. Grueter B, et al. Runx3 regulates integrin αE/CD103 and CD4 expression during development of CD4−/CD8+ T cells. J Immunol. 2005; 175:1694–1705. [PubMed: 16034110]
23. Lotem J, et al. Runx3-mediated transcriptional program in cytotoxic lymphocytes. PloS one. 2013; 8:e80467. [PubMed: 24236182]
24. Reis BS, van Konijnenburg DPH, Grivennikov SI, Mucida D. Transcription factor T-bet regulates intraepithelial lymphocyte functional maturation. Immunity. 2014; 41:244–256. [PubMed: 25148025]
25. Djenidi F, et al. CD8+ CD103+ Tumor–Infiltrating Lymphocytes Are Tumor-Specific Tissue-Resident Memory T Cells and a Prognostic Factor for Survival in Lung Cancer Patients. J Immunol. 2015; 194:3475–3486. [PubMed: 25725111]
26. Ganesan AP, et al. Tissue-resident memory features are linked to the magnitude of cytotoxic T cell responses in human lung cancer. Nat Immunol. 2017; 18:940–950. [PubMed: 28628092]
27. Doedens AL, et al. Molecular programming of tumor-infiltrating CD8+ T cells and IL15 resistance. Cancer Immunol Res. 2016; 4:799–811. [PubMed: 27485135]
28. Gooden MJ, de Bock GH, Leffers N, Daemen T, Nijman HW. The prognostic influence of tumour-infiltrating lymphocytes in cancer: a systematic review with meta-analysis. Br J Cancer. 2011; 105:93–103. [PubMed: 21629244]
29. Singer M, et al. A distinct gene module for dysfunction uncoupled from activation in tumor-infiltrating T cells. Cell. 2016; 166:1500–1511. [PubMed: 27610572]
30. Tirosh I, et al. Dissecting the multicellular ecosystem of metastatic melanoma by single-cell RNA-seq. Science. 2016; 352:189–196. [PubMed: 27124452]
31. Steinert EM, et al. Quantifying Memory CD8 T Cells Reveals Regionalization of Immunosurveillance. Cell. 2015; 161:737–749. [PubMed: 25957682]
32. Benck CJ, Martinov T, Fife BT, Chatterjea D. Isolation of Infiltrating Leukocytes from Mouse Skin Using Enzymatic Digest and Gradient Separation. J Vis Exp. 2016:e53638. [PubMed: 26863129]
33. Knott SR, et al. A computational algorithm to predict shRNA potency. Mol Cell. 2014; 56:796–807. [PubMed: 25435137]
34. Pear WS, et al. Efficient and rapid induction of a chronic myelogenous leukemia-like myeloproliferative disease in mice receiving P210 bcr/abl-transduced bone marrow. Blood. 1998; 92:3780–3792. [PubMed: 9808572]
35. Best JA, et al. Transcriptional insights into the CD8+ T cell response to infection and memory T cell formation. Nat Immunol. 2013; 14:404–412. [PubMed: 23396170]
36. Trapnell C, Pachter L, Salzberg SL. TopHat: discovering splice junctions with RNA-Seq. Bioinformatics. 2009; 25:1105–1111. [PubMed: 19289445]

37. Anders S, Pyl PT, Huber W. HTSeq–a Python framework to work with high-throughput sequencing data. Bioinformatics. 2015; 31:166–169. [PubMed: 25260700]

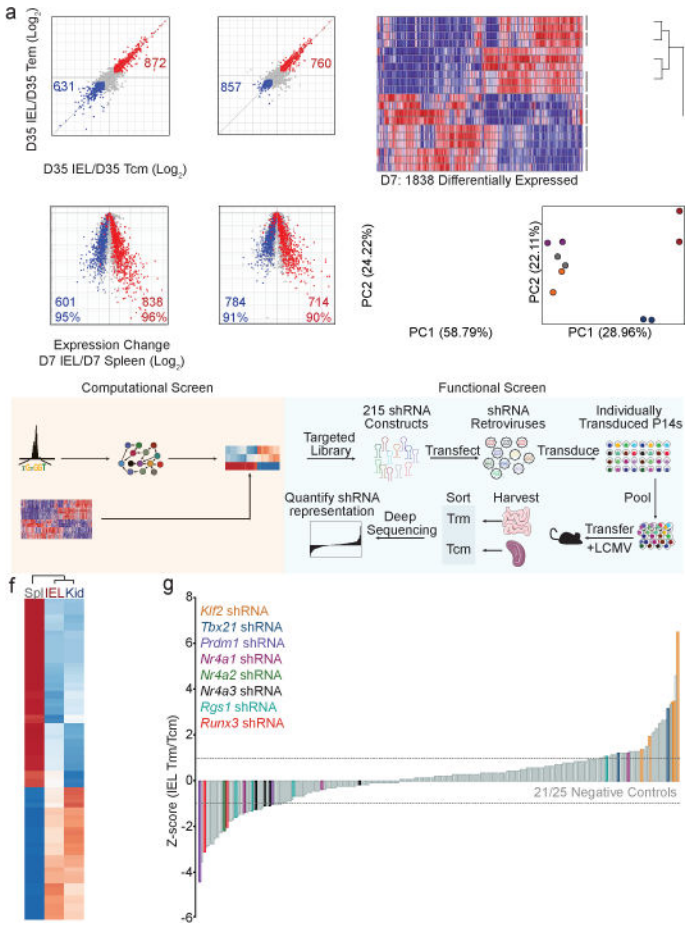

Figure 1.

Computational and functional RNAi screens identify transcriptional regulators of Trm differentiation.

a, Comparison of gene-expression of IEL (left) and kidney Trm (right) relative to Tcm and Tem subsets on day 35 of LCMV infection; red, genes elevated in Trm relative to Tcm and Tem; blue, genes elevated in Tcm and Tem relative to Trm (top). Comparison of differentially-expressed genes in mature Trm (from top panel) in cells from the spleen, IEL, or kidney on day 7 of infection (bottom). **b**, Differentially-expressed genes between splenic, IEL, and kidney populations on day 7 of infection were compared among effector and memory $CD8^+$ T cell subsets. Populations are ordered by hierarchical clustering with Pearson correlation. **c**, PCA of differentially-expressed genes among day 7 subsets and naive P14 cells. **d**, PCA of differential global chromatin accessibility of subsets on day 7 of infection identified by ATAC-seq analysis. **e**, Combinatorial screening approach. **f**, TFs with a PageRank score of ≥1.5-fold change in day 7 non-lymphoid cells compared to day 7 splenic cells are included in the heatmap; genes known to regulate Trm formation are in bold font. **i**, Relative enrichment of shRNAmirs in IEL Trm relative to splenic Tcm from the RNAi screen, reported as the average Z-score from 3 independent screens where each independent screen was performed by pooling DNA from sorted P14 cells from 15–18 mice. Each timepoint represents an individual experiment consisting of 2–3 biological replicates where n=2–10 mice were pooled for each replicate (**a–d**).

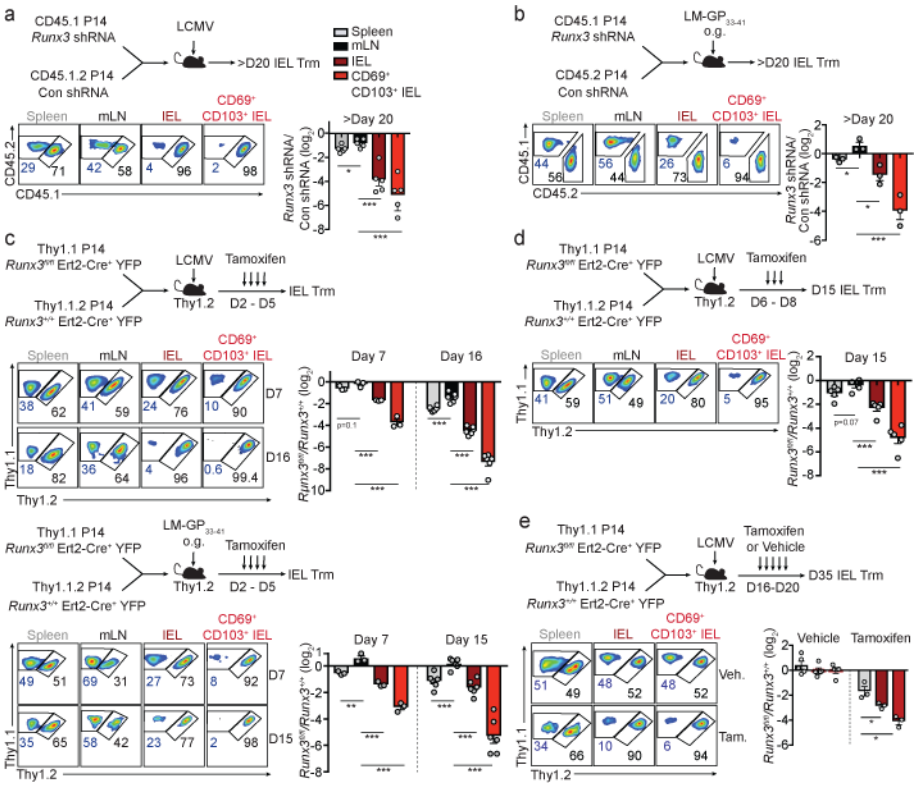

Figure 2.

Runx3 is essential for the differentiation and long-term maintenance of CD8$^+$ Trm cells. **a**, Ratio of *Runx3*- or control-shRNAmir transduced P14 cells in indicated tissues on day 23 or 26 of LCMV infection. **b**, Ratio of transduced transferred cells in indicated tissues on day 32 of enteric LM-GP$^{33–41}$ infection. **c**, Ratio of transferred *Runx3*$^{fl/fl}$Ert2-Cre$^+$YFP (*Runx3*$^{fl/fl}$) and *Runx3*$^{+/+}$Ert2-Cre$^+$YFP (*Runx3*$^{+/+}$) P14 cells in indicated tissues on days 6/7 and 15/16 of LCMV infection (top) or enteric LM-GP$^{33–41}$ infection (bottom). **d**, Ratio *Runx3*$^{fl/fl}$ and *Runx3*$^{+/+}$ P14 cells on day 15 of LCMV infection. **e**, Ratio of *Runx3*$^{fl/fl}$ and *Runx3*$^{+/+}$ P14 cells on day 35 of infection. Graphs indicate mean ± s.e.m of n=5 (**a**), n=3 (**b**), n=3 (day 7) and n= 6 (day 15/16) (**c**), n=5 (**d**), and n=5 (vehicle) and n=3 (tamoxifen) (**e**). All data are from one representative experiment of 2 independent experiments except **a** is pooled from 2 independent experiments; *P<0.05, **P<0.01, ***P<0.005. Symbols represent an individual mouse (**a–e**).

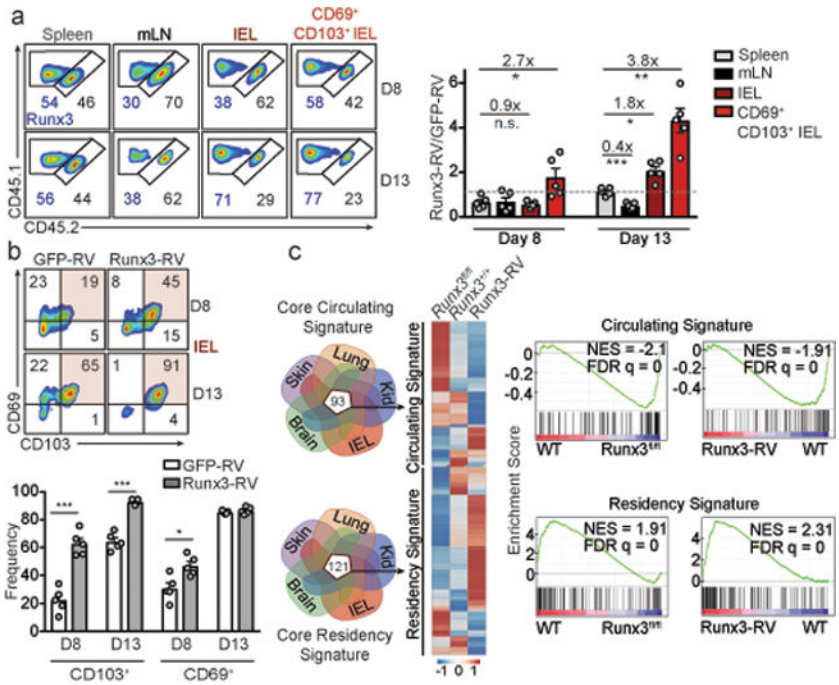

Figure 3.

Runx3 programs CD8$^+$ T cell tissue-residency.

a, Congenically distinct P14 cells were transduced with Runx3-RV (CD45.1$^+$ cells) or GFP-RV (CD45.1.2$^+$ cells), mixed at a 1:1 ratio, and transferred to recipient mice subsequently infected with LCMV. Ratio of transduced cells evaluated on days 8 and 12/13 of infection. **b** Frequency of CD69$^+$ and CD103$^+$ cells from **a**. **c**, Relative expression of the core "circulating" and "residency" genes between Runx3-RV, *Runx3$^{fl/fl}$*, and *Runx3$^{+/+}$* CD8$^+$ T cells (left) and gene set enrichment analysis (right). Graphs show mean ± s.e.m of n=5 mice (**a**,**b**) from one representative experiment of 2 independent experiments, *P<0.05, **P<0.01, ***P<0.005, n.s., not significant. Symbols represent an individual mouse (**a,b**).

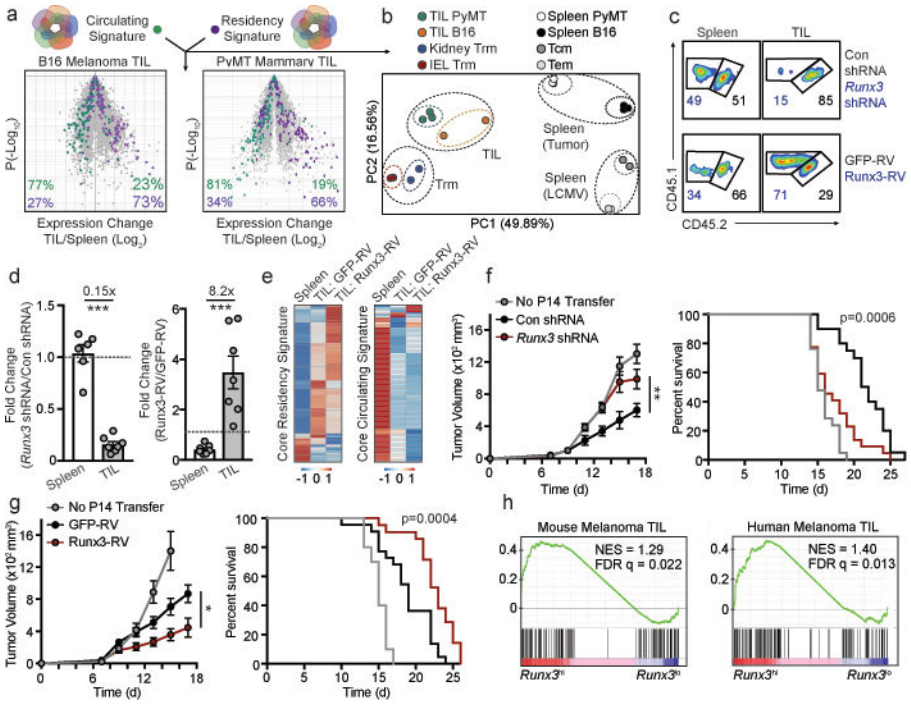

Figure 4.

CD8$^+$ TIL share transcriptional similarity with Trm and require Runx3 for tumor residency. **a**, Comparison of the core tissue-residency signature and core circulating signature (from Fig. 3c) in B16 melanoma CD8$^+$ TIL[27] or PyMT mammary tumor CD8$^+$ TIL[27] relative to corresponding splenic cells. **b**, PCA of gene-expression of the core tissue-residency and circulating gene sets for TIL, Trm, or splenic subsets. **c**, **d** Congenically distinct P14 cells were transduced with *Runx3* shRNAmir or Runx3-RV (CD45.1$^+$ cells) and Con shRNAmir or GFP-RV (CD45.1.2$^+$ cells), mixed at a 1:1 ratio and transferred into mice with established B16-GP$^{33–41}$ melanoma tumors. Flow plots and graphs indicate ratio of transduced cells. **e**, Relative expression of the core tissue-residency and core circulating gene sets in GFP-RV splenocytes, GFP-RV TIL, and Runx3-RV TIL following the same approach as in **c**. **f**,**g**, Tumor growth and survival following adoptive transfer of the indicated cell population. **h**, Gene set enrichment analysis of the core tissue-residency signature in *Runx3*^{hi} vs *Runx3*^{lo} TIL from single-cell RNA-seq analyses of mouse[29] and human[30] melanoma TIL. Graphs indicate mean ± s.e.m of n=5 (*Runx3* shRNAmir) or n=7 mice per group (Runx3-RV) from one representative experiment of 3 independent experiments (**c**,**d**) or data pooled from 3 independent experiments consisting of n=10–21 mice per group (**f**, **g**), *P<0.05, **P<0.01, ***P<0.005. Symbols represent an individual mouse (**d**).